

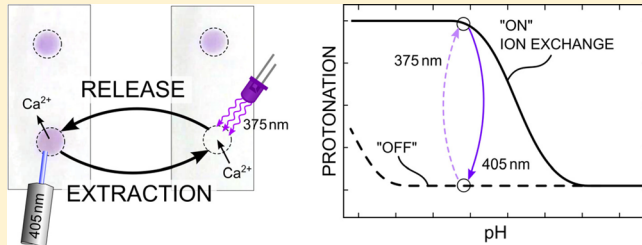
# Photoresponsive Ion Extraction/Release Systems: Dynamic Ion Optodes for Calcium and Sodium Based on Photochromic Spiropyran

Günter Mistlberger,\* Xiaojiang Xie, Marcin Pawlak, Gastón A. Crespo, and Eric Bakker\*

Department of Inorganic and Analytical Chemistry, University of Geneva, 30 Quai Ernest Ansermet, 1211 Geneve 4, Switzerland

 [Supporting Information](#)

**ABSTRACT:** Photoresponsive ion extraction/release systems (PRIONERS) represent a highly interesting tool for the localized and time-controlled chemical perturbation of biological materials. We report here on our first results on phototriggered calcium and sodium exchanging materials. Such materials exist in two distinct states (“on” and “off”), depending on the wavelength of illumination. We used a combination of spectroscopic and electrochemical methods to obtain a better understanding of the dynamic processes involved in the triggered ion-exchange reaction upon activation of the photoactive compound. The driving force for the ion exchange is the light-induced acidity change of the chromoionophore. Activation with UV light generates a species in the membrane with an increased  $pK_a$ . Protons are pulled into the membrane, and at the same time, ions are expelled. The selectivity of the system is determined by the employed ionophore. In contrast to photoresponsive ionophore-based systems, the concept presented here is applicable for virtually any ion of interest for which an ionophore exists.



Ion optodes based on the competitive ion exchange between a hydrophobic sensor phase and an aqueous sample solution were widely applied since their introduction in the late 1980s.<sup>1–9</sup> In cases where the ionophore or analyte ion carrier is silent concerning the optical response to a binding event, one can take advantage of a secondary reporter dye. Here, the protonation degree of the reporter dye indirectly monitors the concentration of the analyte in the membrane phase, as the sensing phase must obey the electroneutrality principle. This is an elegant approach because it enables the measurement of various ions using their respective ionophores with the same reporter dye and optical setup. On the other hand, one can tune the response region from trace level sensing to completely nonresponsive systems by choosing the indicator of the respective  $pK_a$ .<sup>10</sup> After the preparation of the sensor, however, the response function is fixed given that the nature and total concentration of all components remains constant.

Replacing one of the sensor components with a dynamically changeable version of the component will transform such sensors from passive to dynamic devices.<sup>11</sup> The triggered change of the affinity of the ionophore, the charge of the ion exchanger, or the  $pK_a$  of the indicator will suddenly allow for a controlled change in sensor characteristics in space and time. While light is most often used for triggering such reactions, other stimuli, such as heat,<sup>12</sup> mechanical stress,<sup>13</sup> and electrical activation<sup>14</sup> have been reported. The advantage of using light is the relative ease of combining spatial and temporal control of the trigger by using readily available imaging equipment such as microscopes or spectrometers.

We recently reported on the photoinduced acidity change of a derivative of the photochromic dye spirobifluorene inside plasticized PVC membranes.<sup>15</sup> This was the first example where the  $pK_a$  change of the indicator was suggested as the driving force for a change in equilibrium conditions of an ion-sensing membrane. We subsequently demonstrated the proof of concept by using an anion sensor based on the coextraction of protons and chloride into a lipophilic membrane.<sup>16</sup> The ultimate goal, however, would be a system that can release and extract specific ions in a highly controlled manner. Calcium, for instance, plays a crucial role in biology and is involved in the control of such diverse processes as fertilization, proliferation, development, learning and memory, contraction and secretion, necrosis, and apoptosis.<sup>17,18</sup>

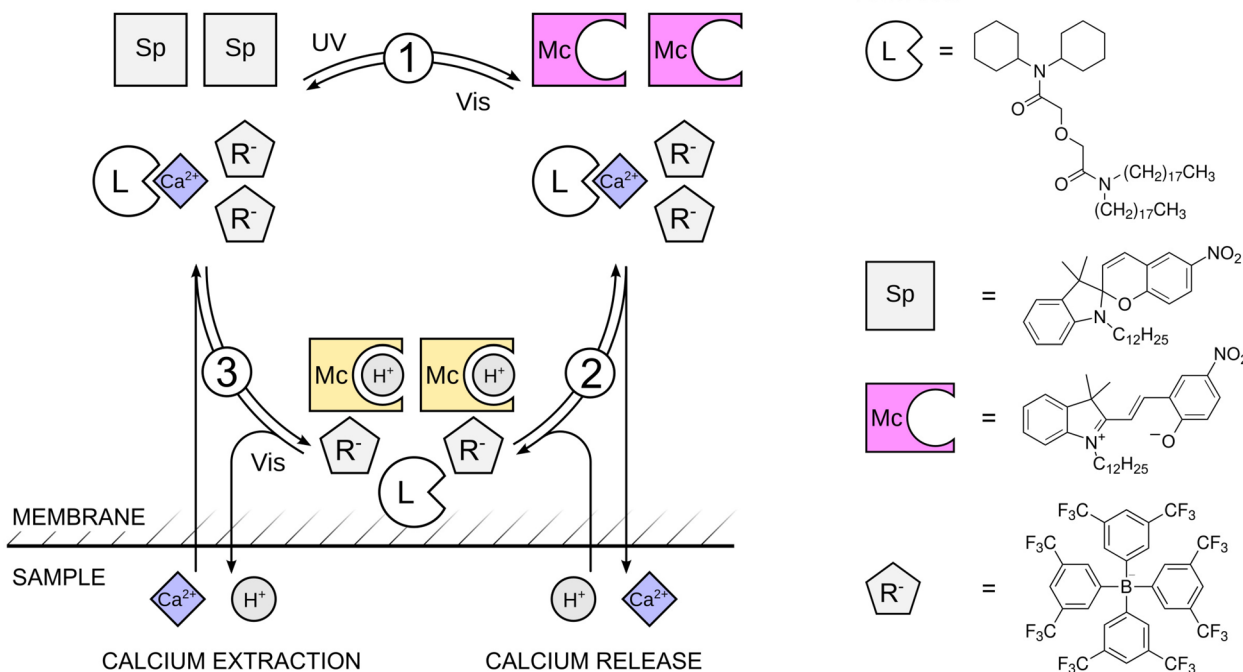
Photorelease of small ionic species was reported for protons based on photoacid generators<sup>19</sup> or the photoisomerization of organic compounds.<sup>20,21</sup> For other ionic species photoactive chelating compounds were used for reversible<sup>22–25</sup> and irreversible affinity changes (photo cages).<sup>26</sup> In our work, however, the driving force for triggered ion exchange is the change in  $pK_a$  of a photoactive chromoionophore. This approach is more flexible than the previous one, because the same photoactive compound can be used for producing photoresponsive ion extraction/release systems (PRIONERS).

**Received:** January 9, 2013

**Accepted:** February 7, 2013

**Published:** February 7, 2013

**Scheme 1.** Schematic Representation of the Sequence of Processes Involved in the Photoactivated Ion Release Explained by Example of a Calcium-Selective Membrane



with selectivity toward any ion of interest for which an ionophore is available.

Here, we report on our first results on calcium and sodium-selective PRIONERS based on spiropyran, a well-known photochromic dye that was previously employed in photoswitchable devices<sup>27–30</sup> (Scheme 1). In its original state spiropyran (Sp) exists in its ring-closed form with a low  $pK_a$  (1).<sup>15</sup> UV illumination generates the ring-opened merocyanine form (Mc), which exhibits a much higher  $pK_a$  (2). Due to this change in acidity, the previously passive sensor becomes active by allowing the exchange of protons and analyte ions with the contacting sample solution (3). Finally, the inactive state can be restored by illumination with visible light. Due to the huge, phototriggered shift in  $pK_a$  of the involved indicator, the response curve of such a sensing phase toward changes in proton or ion activity shifts as well (Figure 1). Therefore, a sensor built in this way can be completely switched on or off depending on the wavelength of the light used for illumination, or an ion extraction/release can be initiated using light. This leads to a range of novel possibilities in the optical determination and manipulation of ion concentrations. In principle, switchable sensors allow for the modulation of a sensor signal which facilitates the background correction in optical detection. Moreover, the dynamic response of the sensor may reveal certain information about the microenvironment of the sensor and the speciation of the analyte. Finally, contact between analyte and active components may be blocked in the off state.<sup>16</sup> This allows a clear separation of the sensor delivery stage from the actual read-out stage. Fluorescence and potentiometric measurements showed the change in response behavior depending on wavelength of the light used for illumination. Despite the fact that the switching process of the photoactive compound is a dynamic process with a change of the concentrations of species inside the membrane, the calibration and selectivity data fit well to the theoretical

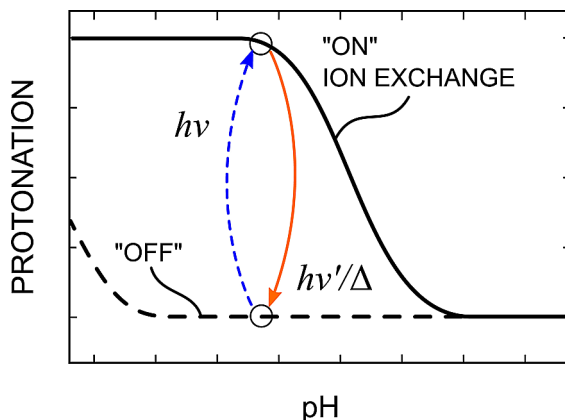


**Figure 1.** Schematic representation of the photoinduced change of an optode response function. Depending on the location of the two response curves and the sample pH, a total or partial ion exchange occurs upon activation.

response described for equilibrium-based optodes. Moreover, it was possible to visualize the change in the response function using a special flow cell for simultaneous electrochemical and optical characterization of optode membranes. Finally, for naked eye detection, such sensors might be switched on or off using low-cost optical devices such as a UV-LED and a laser pointer.

## EXPERIMENTAL METHODS

**Chemicals and Membrane Preparation.** Details on the employed chemicals and the membrane preparation process can be found in the Supporting Information. Briefly, all membranes were based on plasticized poly(vinyl chloride) (PVC). The membranes for optical characterization were spin coated onto poly(ethylene terephthalate) (PET) foils, while membranes for potentiometric characterization were produced

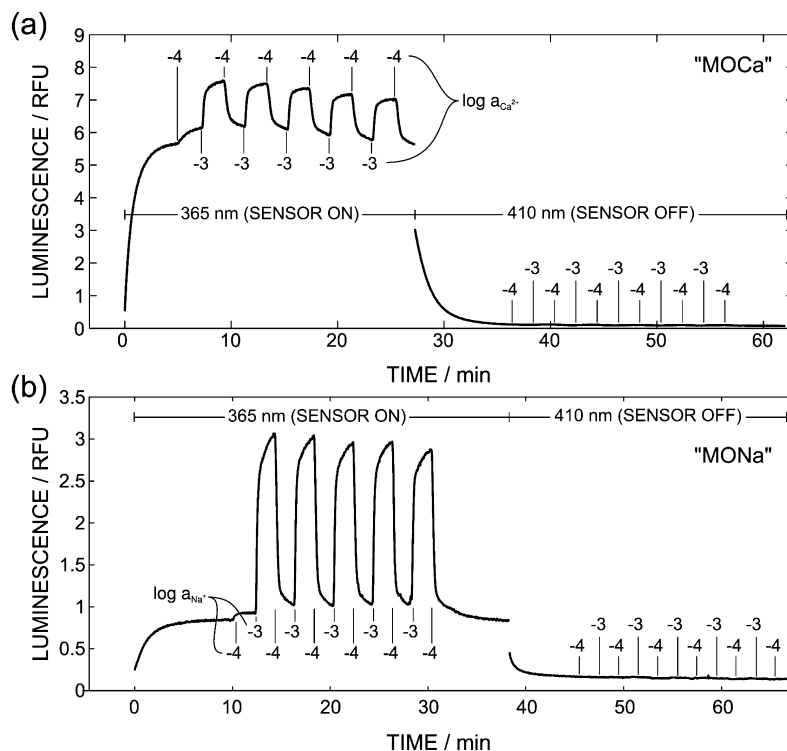


**Figure 2.** Comparison of the sensor response of a MOCa (a) and a MONa membrane (b) to two different analyte concentrations when activated with 365 nm light (“on” state) and under illumination with 410 nm light (“off” state). Both examples show clearly that there is no measurable response in the “off” state while the activated sensor responds to a change in analyte concentration as expected for a conventional ion-selective bulk optode.

using conventional solvent casting techniques in a glass ring. The three different membranes are referred to as “MOCa” (optical characterization, calcium selective), “MONa” (optical characterization, sodium selective), and “MPCa” (potentiometric characterization, calcium selective).

**Obtaining the Optical Response Function.** One of the coated PET foils was placed in a screw-capped, semimicroscale fluorescence quartz cell. The cell was closed with a silicone septum, placed into the fluorescence spectrometer (Fluorolog3, Horiba Jobin Yvon), and utilized as a flow cell by circulating the sample solution with a peristaltic pump (Gilson Minipuls3), thereafter. The measurements were carried out in 0.01 M formic acid buffered solutions (pH 3.6) for calcium-selective membranes and 0.01 M Tris–HCl buffered solutions (pH 7.2) for sodium-selective membranes. The membranes were activated by setting the excitation monochromator to 365 nm with a 0.5 nm slit width in order to minimize photobleaching during the measurement. The emission was recorded at 650 nm. The fluorescence values for the fully protonated and deprotonated states were obtained by adding 1 M H<sub>2</sub>SO<sub>4</sub> and 2 M NaOH, respectively, until no further change in signal was detected.

**Simultaneous Potentiometric and Optical Measurements.** Potentiometric measurements were carried out using an improved version of a previously described flow cell.<sup>15</sup> Further details on the measurement setup, a discussion of the improvements over the previous version, and a schematic representation of the flow cell are provided in the Supporting Information.

## RESULTS AND DISCUSSION

In Figure 2 the optical response of calcium-selective (Figure 2a) and sodium-selective (Figure 2b) membranes to changes in the concentration of the respective primary ions is shown. The membranes were first activated by illuminating at 365 nm, and once the signal was stable, the flow cell was flushed alternately with solutions containing 10<sup>-4</sup> and 10<sup>-3</sup> M Ca<sup>2+</sup> (five cycles, 120 s per step, pH 4.0). The recorded emission at 650 nm is a measure for the protonation degree of Mc, where Mc emits more strongly than McH<sup>+</sup>. The reversible change of the intensity suggests that the membrane in the on state seems to work as a conventional ion-selective bulk optode. Afterward, the wavelength of the illumination source was changed to 410 nm, which pushes the Mc form toward the Sp form, but still allows for the measurement of the fluorescence emission of Mc. The membranes returned to the off state (Mc → Sp), and there was practically no response toward changing calcium concentrations. The same was true for a sodium-selective membrane, as shown in Figure 2b (pH 7.0). The slightly longer response time of this membrane revealed an increased membrane thickness resulting from the differences in cocktail composition, mainly the use of tetrahydrofuran instead of cyclohexanone as casting solvent.

These plots also reveal the small but nevertheless significant drift of the signal over time. We tried to minimize the light intensity during interrogation in order to minimize photobleaching of the Sp; however, this also required more time for sensor activation. For the final application, which includes the intracellular delivery of small ionic species, the light density will be much higher due to the focusing of high-power light sources such as lasers onto a small sample volume. Ultimately, the optimum light intensity will depend on the specific require-

ments of an experiment, especially considering long-term stability and speed of action.

The time required for switching the sensor obviously depends on the illumination intensity. Increasing the light intensity 70 times compared to the intensity used for the measurements in Figure 2 reduced the switching times to 15 s for the on state and 60 s for off (see inset, Figure 3). On the

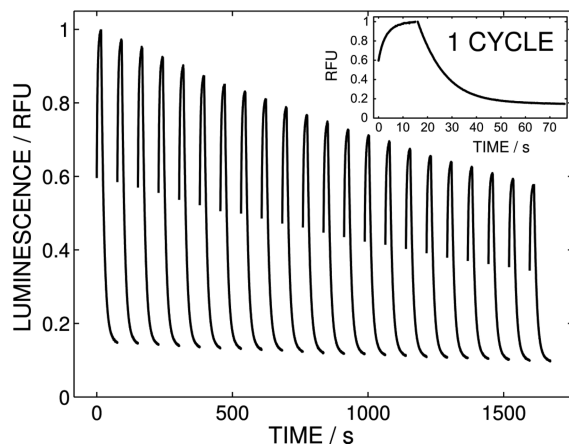


**Figure 3.** Repeated cycles of activation (15 s,  $\lambda_{\text{ex}} = 365 \text{ nm}$ ) and deactivation (60 s,  $\lambda_{\text{ex}} = 410 \text{ nm}$ ). While the time for activation under these conditions is relatively fast, it is clearly visible that the 22 cycles for full activation and deactivation result in significant signal loss of about 40%.

downside, this also increases the effect of photobleaching. Twenty-two full switching cycles under these conditions reduced the luminescence intensity by approximately 40%. For this study of selectivity and ion-exchanging properties, the photostability was not a major issue due to the conversion of the output signal to protonation degree for quantitative evaluation. For delivery systems with sufficient photostability for medium to long-term studies, however, a photoactive compound with increased photostability would be desirable. This issue is currently under investigation in our laboratory.

In order to get a better understanding of the processes involved during the phototriggered  $pK_a$  change of a chromoionophore inside a cation-selective bulk optode, we characterize membranes with compositions common for calcium-selective optodes. The response of such a calcium-selective optode membrane (MOCa) toward changing concentrations of  $\text{Ca}^{2+}$  and the interfering ions  $\text{Mg}^{2+}$ ,  $\text{K}^+$ , and  $\text{Na}^+$  is shown in Figure 4. The slow but significant photobleaching during the time required for calibration made it necessary to perform a simple baseline correction of the measured signal. The signal represents the emission intensity at 650 nm after activating the sensor at 365 nm and subtracting the baseline. Magnesium ions started to interfere at 0.25 mM, while sodium and potassium were unable to compete with protons bound to the indicator dye throughout the tested range.

The actual position of the baseline does not affect the calibration because the emission intensity is transformed to values for the protonation degree  $1 - \alpha$ . After measuring the values for  $F_{\min}$  and  $F_{\max}$  which are the fluorescence emission of fully protonated ( $\text{McH}^+$ ) and fully deprotonated ( $\text{Mc}$ ) spiropyran, respectively, the protonation degree  $1 - \alpha$  was calculated using the relationship

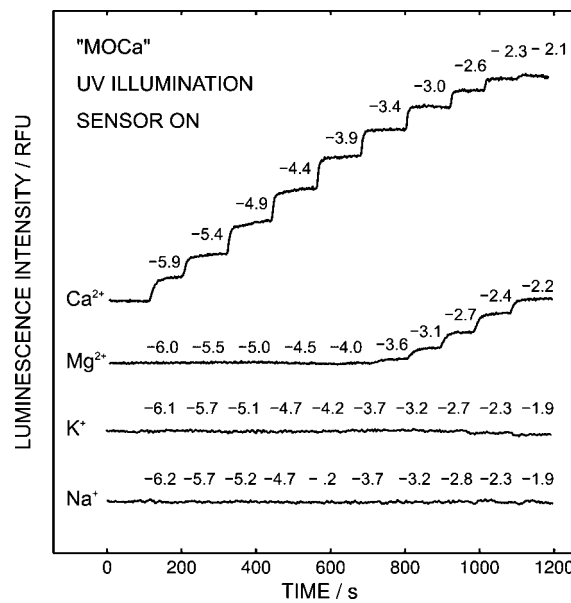
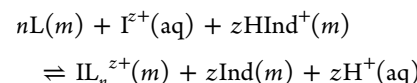


**Figure 4.** Response of a calcium-selective optode in the activated state toward different concentrations of analyte and interfering ions. The signal is the luminescence emission measured at 650 nm under constant illumination of the sensor with light of 365 nm.

$$1 - \alpha = \frac{F_{\max} - F}{F_{\max} - F_{\min}} \quad (1)$$

where  $F$  is the emission intensity at 650 nm at a given analyte concentration.

Assuming that the concentration of interfering ions is negligible, the optode response can be described with the following general equilibrium:



where L represents the ionophore, HInd and Ind are the concentration of protonated and deprotonated indicator,  $z$  is the charge of the ion of interest, and  $n$  is the complex stoichiometry. The exchange constant for this equilibrium is given by

$$K_{\text{exch}}^{\text{IL}_n} = \frac{[\text{L}_n\text{I}^{z+}][\text{Ind}]^z (a_{\text{H}^+})^z}{[\text{L}]^n [\text{HInd}^+]^z a_{\text{I}^{z+}}} \quad (2)$$

where values in square brackets represent the concentrations in the membrane and  $a_{\text{H}^+}$  and  $a_{\text{I}^{z+}}$  are the activities of protons and analyte ions in the contacting sample solution. From eq 2 the optode response function for the activity of the primary ion can be derived using mass and charge balances and the protonation degree of the indicator (see the Supporting Information for details):

$$\begin{aligned} a_{\text{I}^{z+}} &= \frac{(a_{\text{H}^+})^z}{zK_{\text{exch}}^{\text{IL}_n}} \left( \frac{\alpha}{1 - \alpha} \right)^z (R_T - (1 - \alpha)\text{Ind}_T) \\ &\quad \left( L_T - \frac{n(R_T - (1 - \alpha)\text{Ind}_T)}{z} \right)^{-n} \end{aligned} \quad (3)$$

where  $L_T$ ,  $R_T$ , and  $\text{Ind}_T$  are the total molar concentrations of ionophore, ion exchanger, and indicator in the membrane. Plotting the values for  $1 - \alpha$  versus the logarithmic activity of the sample solution  $\log a_{\text{I}^{z+}}$  resulted in the calibration plot

shown in Figure 5. Small differences in the pH values were corrected by normalizing to pH 3.6 according to Lerchi et al.<sup>10</sup>

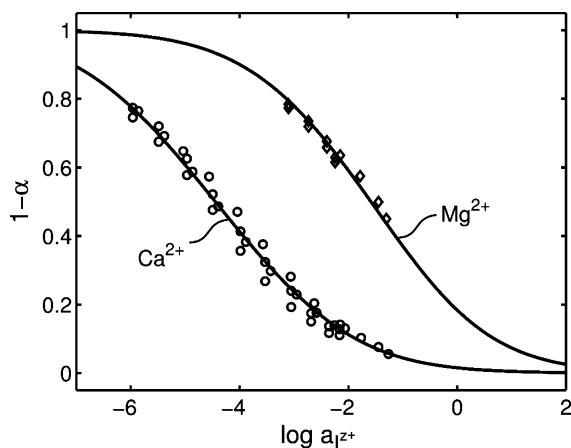


**Figure 5.** Calibration curves of a photoactivated calcium-selective optode. Sodium and potassium did not give a measurable response.

Fitting the data with the optode response function resulted in the values for  $\log K_{\text{exch}}^{\text{IL}_n}$  of  $-0.7 \pm 0.1$  ( $n = 3$ ) for  $\text{Ca}^{2+}$  and  $-5.1 \pm 0.1$  ( $n = 2$ ) for  $\text{Mg}^{2+}$ . The complex stoichiometries were assumed to be 3 for calcium and 2 for magnesium.<sup>31,32</sup>

Finally, the selectivity  $\log K_{ij}^{\text{opt}}(\text{SSM})$  can be calculated according to Bakker et al.<sup>2</sup> (Supporting Information). The value was calculated for  $1 - \alpha = 0.5$  and resulted in a  $\log K_{\text{Ca},\text{Mg}}^{\text{opt}}(\text{SSM}) = -2.9 \pm 0.2$ . This means that calcium will be preferred over magnesium by roughly 3 orders of magnitude. This is an important fact for the selectivity of the release in a biological system. A high selectivity ensures that, for instance, calcium-loaded particles cannot exchange their load with magnesium during particle delivery even when being exposed to cell compartments with higher magnesium concentrations. Only the phototriggered  $pK_a$  change of the indicator will allow the exchange of protons for calcium ions. The selectivity over potassium and sodium is even better with  $\log K_{ij}^{\text{opt}}(\text{SSM})$  smaller than  $-8.9$  for potassium and  $-6.6$  for sodium.

Employing the indicator as the photoactive compound instead of the ionophore has the big advantage that the tedious development, optimization, and characterization of a photoactive substance only needs to be done once. Afterward, one and the same compound can be used to implement all kinds of different ion extraction/release systems by simply changing the ionophore and/or ion exchanger. As a demonstration of this concept we prepared a membrane containing the same amount of Sp but instead of Ca-ionophore IV we included Na-ionophore X. The data of the separate solution method for this membrane is shown in Figure 6 and demonstrates that the film can now be loaded with sodium with a high selectivity over potassium, magnesium, and calcium ions. The values for  $\log K_{ij}^{\text{opt}}(\text{SSM})$  with sodium as the primary ion are  $-2.4$ ,  $-4.0$ , and  $-4.1$  for potassium, calcium, and magnesium, respectively. While the sodium selectivity of such a photorelease system over calcium and magnesium is sufficient considering normal intracellular concentration levels, the potassium/sodium ratio inside cells is probably too high to completely suppress premature sodium release due to exchange with potassium using Na-ionophore X. This may be solved by using an ionophore with a higher selectivity, such as a 1,3-bridged calix[4]arene derivative described in the literature.<sup>33,34</sup>

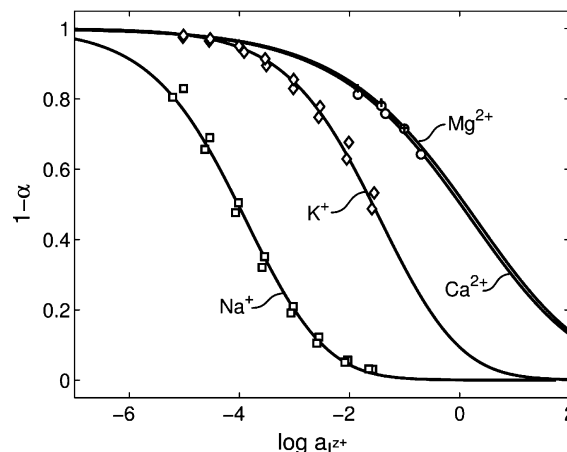


**Figure 6.** Calibration curves of a photodynamic, sodium-selective optode membrane.

As shown in Figure 2, the MOCa and MONa membranes can be switched on and off depending on the wavelength of the light used for illumination. Although the membranes in the on mode responded as expected to changing analyte concentrations, the optical experiment is no proof for the absence of exchange between protons and analyte ions in the off state. The reason for this is the spectral similarity of spiropyran in the protonated  $\text{SpH}^+$  and the deprotonated Sp form.<sup>15</sup> In other words, even if a change in calcium or proton concentration would change the protonation degree of Sp, the change would be invisible. For this reason we had to rely on a different method to substantiate that the photoresponsive membrane in the off state does not permit ion exchange between protons and analyte ions. On the basis of our previous experience, we decided for potentiometry as the method of choice. We prepared membranes containing Sp, Ca-ionophore IV, and NaTFPB and characterized their potential response to pH at different calcium background concentrations in both off and on states. The results in Figure 7 show that below a certain pH the membrane in the on state starts to exchange protons with the contacting sample solution, resulting in a Nernstian response toward proton activity. In the off state, there is no response to a changing proton concentration throughout the tested range, which indeed suggests that protons cannot compete with  $\text{Ca}^{2+}$  ions due to insufficient affinity of Sp for protons. Above the critical pH, neither Mc nor Sp is protonated and the MPCa membrane behaves as a regular ion-selective electrode membrane by showing a Nernstian response for calcium. In the on state, a selectivity of  $\log K_{\text{H}^+, \text{Ca}^{2+}}^{\text{pot}} = -3.5 \pm 0.1$  was calculated by fitting eq 4 with a fixed theoretical slope of 58.1 mV per decade:<sup>2</sup>

$$\text{EMF} = E_{\text{H}^+}^0 + \frac{RT}{F} \ln \left( \frac{a_{\text{H}^+}}{2} + 0.5 \sqrt{(a_{\text{H}^+})^2 + 4a_{\text{Ca}^{2+}}(K_{\text{H}^+, \text{Ca}^{2+}}^{\text{pot}})^2} \right) \quad (4)$$

The raw data of the combined optical–electrochemical measurement shown in Figure 8 gives some insight in the complexity of the processes involved in these measurements. The sequence of events during the calibration can be summarized in the following way (see the inset in Figure 8): (1) solution flow through the cell is stopped (“PUMP OFF”), (2) begin of illumination at 365 nm (“UV”), (3) change of

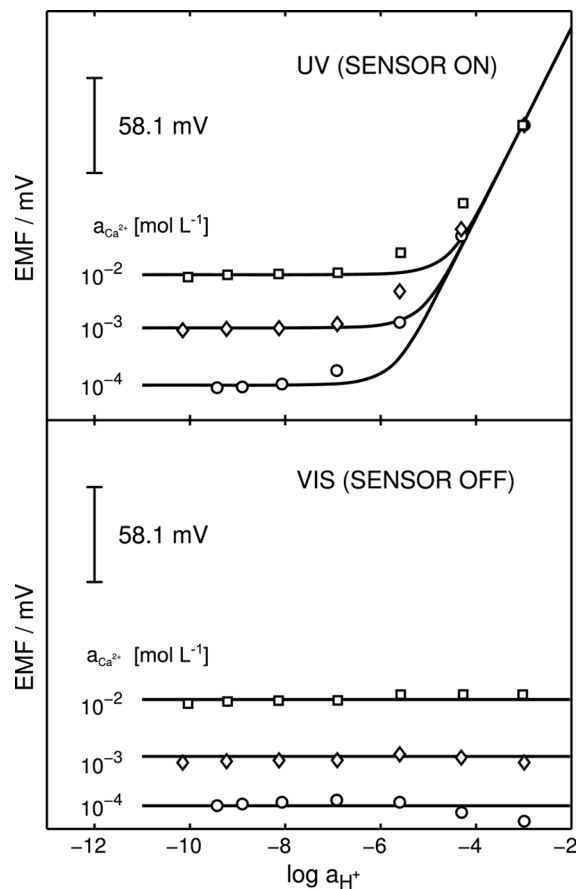


**Figure 7.** Potentiometric response of a calcium-selective membrane (MPCa) to changing proton and calcium activities in on and off state.

wavelength to 410 nm (“VIS”), and (4) start of flow through sample compartment with next sample solution (“PUMP ON”). When the EMF response (upper plots) and the luminescence emission at 650 nm (lower plot) are compared, it is obvious that only the membrane potential is significantly affected by the changes in pH and  $a_{\text{Ca}^{2+}}$ . This is expected because the ion-exchanger concentration is lower than the

concentration of indicator dye, and therefore, even at very low pH the permselectivity of the membrane prohibits a protonation degree higher than 10%. On the other hand, it is surprising that there seems to be almost no photobleaching present in this membrane, especially because the illumination was carried out at maximally opened excitation slits in order to achieve fast on/off cycles. This can be explained by the increased thickness of the membrane, which has two different effects. First, the increased volume of the membrane may act as a reservoir of dye. This means that a concentration gradient of dye caused by bleaching will be partly compensated by diffusion of dye from the backside of the membrane or nonilluminated regions. Second, a decrease of the Mc concentration close to the front side of the membrane will expose deeper lying layers of the membrane for illumination because the Mc form has a higher absorption coefficient at 365 nm than the Sp form, and once it is gone, the excitation light can penetrate deeper into the membrane. The dynamics of the EMF signal also gives a hint that these diffusion processes and concentrations gradients inside the membrane may result in pH and analyte activity dependent surface effects. A close comparison of the EMF curves for pH 8.9 and 3.0 at  $10^{-4}$  M  $\text{Ca}^{2+}$  indicates that the speed of both activation (365 nm) and relaxation (410 nm) are faster at lower pH in the contacting solution on the front side of the membrane. Interestingly, at pH 3, the visible light illumination even leads to an “overshooting” of the potential change which then returns to the baseline. This clearly indicates that dynamic processes occur in the membrane and the system cannot strictly be regarded as a totally equilibrated system.

A further indication of this nonequilibrium state is the deviation of the experimental data from the theoretical response function for protons as primary ions and divalent interfering ions in the intermediate region between calcium and proton selectivity (see Figure 7).<sup>2</sup>

Finally, it is also possible to calculate a value for  $\log K_{ij}^{\text{pot}}$  by using the values for  $K_{\text{exch}}$  obtained from the optical selectivity measurements using the following equation:<sup>2</sup>

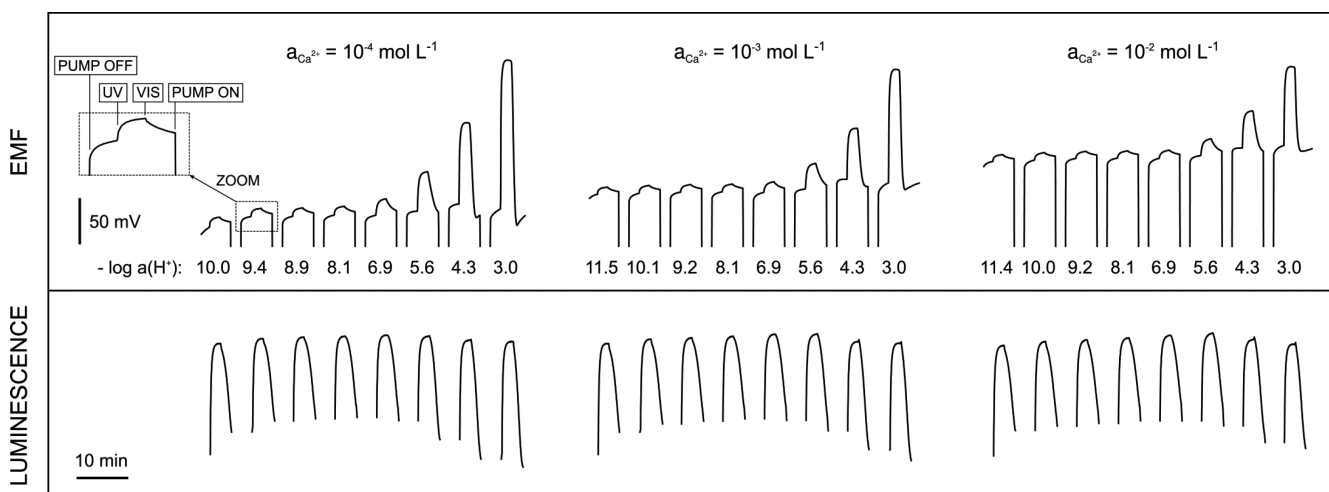


**Figure 8.** Comparison of the potentiometric response with the luminescence of Mc vs time. While the potentiometric signal is influenced by both the pH and calcium concentration in the test solution, the luminescence signal demonstrates that the bulk of the membrane is only affected by the illumination but not the conditions in the contacting solutions.

$$K_{\text{H}^+, \text{Ca}^{2+}}^{\text{pot}} = K_{\text{exch}}^{\text{opt}} \frac{[\text{HInd}^+(\text{H}^+)]}{[\text{Ind}(\text{H}^+)]} \left( \frac{[\text{L}(\text{Ca}^{2+})]^3}{[\text{CaL}_3^{2+}(\text{Ca}^{2+})]} \right)^{1/2} \quad (5)$$

where the notations in parentheses, i.e.,  $(\text{H}^+)$  or  $(\text{Ca}^{2+})$ , mean that these values are acquired under conditions where only the denoted ion can enter the membrane, i.e., the regions showing Nernstian response toward the respective ions. The final equation for  $\log K_{\text{H}^+}^{\text{pot}}$  can be derived as described in the Supporting Information. The resulting value of  $\log K_{\text{H}^+}^{\text{pot}}$  (from opt) = −2.5 is significantly different from the value obtained from the potentiometric measurement ( $\log K_{\text{H}^+}^{\text{pot}}$  (from EMF) = −3.5). Although there is a difference in ionic strength of the contacting solution by a factor of more than 3, this cannot explain the deviation sufficiently. A possible explanation is the difference in membrane composition: in the equilibrium state at  $1 - \alpha = 0.5$  the ratio of free ionophore to complex bound ionophore is 3:1 in the MOCa membrane, whereas it is 1:1 in the Nernstian response region of the MPCa membrane. Moreover, there is a massive difference in the total concentration of the compounds in the membranes, i.e., 12:1 for R and 10:1 for L, respectively (MOCa to MPCa). A subtle change in the equilibrium state between the two experimental cases is therefore possible and may explain the difference in membrane selectivity.

In order to demonstrate a simple example for rapid naked eye detection of calcium with a switchable sensor (Figure 9), we prepared a  $3 \times 4$  array of spots with two different kinds of cocktails. Cocktail A contained  $0.02 \text{ mol kg}^{-1}$  Sp,  $0.024 \text{ mol kg}^{-1}$  NaTFPB, and  $0.06 \text{ mol kg}^{-1}$  Ca-ionophore IV in bis(2-ethylhexyl) sebacate (DOS), whereas cocktail B missed the ionophore but was otherwise the same. One microliter of the cocktail solutions per spot was transferred to a dry filter paper. Afterward, the paper was soaked in Milli-Q purified water. The sensor spots in the original, inactive state are colorless (Figure 9, picture 1). After activation of the optical sensor spots using a low-cost, 375 nm LED, a faint yellow color in all spots became visible, indicating the presence of  $\text{McH}^+$  (Figure 9, picture 2). After changing the calcium concentration in the contacting solution from 0 to  $10^{-3} \text{ M}$  (Figure 9, picture 3), sensor spots containing the ionophore (cocktail A) changed their color from yellow to purple, while the spots without ionophore stayed yellow (Figure 9, picture 4). This means that  $\text{Ca}^{2+}$  entered the cocktail droplets “A”, bound to the ionophore and, at the same time, pushed protons out ( $\text{McH}^+ \rightarrow \text{Mc}$ ). In contrast, spots “B” did not allow the exchange of protons with  $\text{Ca}^{2+}$ , and therefore,  $\text{McH}^+$  persisted. Swiping a beam of a low-cost, 405 nm laser pointer over the two center columns (Figure 9, picture 5) instantly discolored the illuminated spots, indicating the switch from  $\text{Mc}/\text{McH}^+$  to Sp (Figure 9, picture 6). Illumination with the 375 nm LED (Figure 9, picture 7) restored the purple and faint yellow color of the previously deactivated spots, demonstrating that the laser did not bleach the points but deactivated the photoactive compound in a reversible way as outlined in Scheme 1. This is a simple example of how the current system allows for the spatially confined, reversible, and rapid switching of photodynamic sensors. Moreover, low-cost equipment, such as LED and conventional laser pointers, deliver sufficient energy for initiating the reaction.

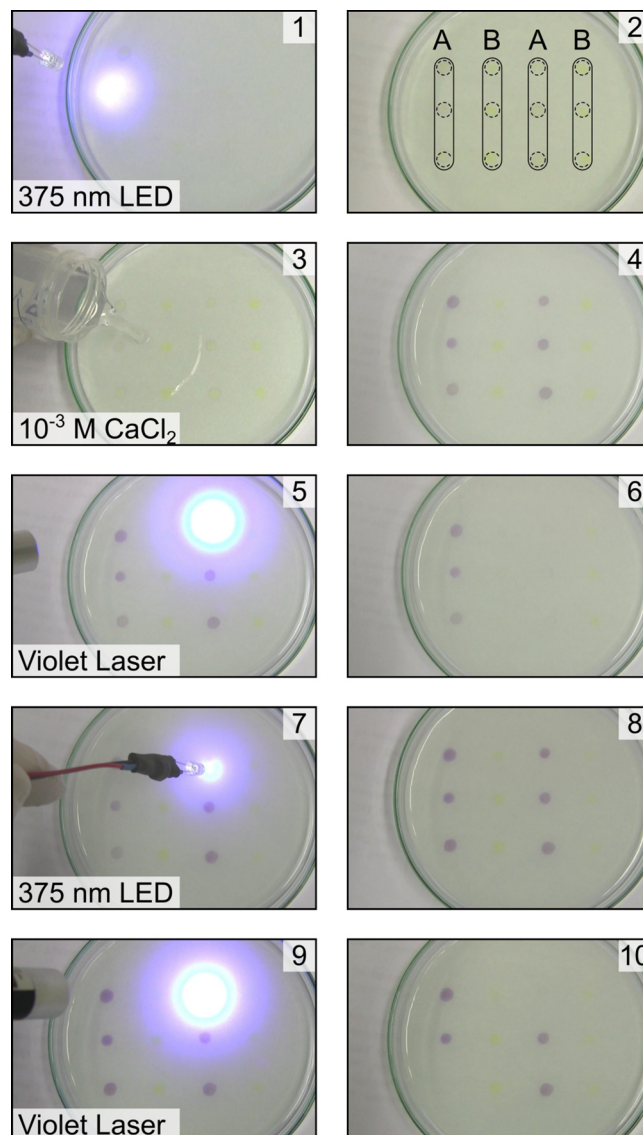


**Figure 9.** Screenshots from a movie demonstrating the reversible switching of optical sensor spots selective for calcium (A) or protons only (B). Switching was carried out with a 375 nm LED (ON) and a 405 nm laser pointer (OFF).

## CONCLUSIONS

Photoresponsive ion extraction/release systems are valuable tools for realizing chemical perturbations of biological species confined in time and space. The thorough study of PRIONERS selective for calcium and sodium ions using both optical and optoelectrochemical methods elucidated the complex dynamic processes involved in such a triggered ion exchange. We were able to demonstrate the selective, triggered exchange of specific ions with the contacting sample solution. The selectivity of both types of PRIONERS was characterized. Finally, we were able to show an illustrative example of how a rapid and simple activation of PRIONERS as sensors can be achieved using low-cost light sources such as laser pointers and LEDs.

## ■ ASSOCIATED CONTENT

### § Supporting Information

Experimental details and derivation of the equations used for evaluation. This material is available free of charge via the Internet at <http://pubs.acs.org>.

## ■ AUTHOR INFORMATION

### Corresponding Author

\*E-mail: eric.bakker@unige.ch (E.B.); g.mistlberger@gmail.com (G.M.).

### Notes

The authors declare no competing financial interest.

## ■ ACKNOWLEDGMENTS

This work was supported by the Swiss National Science Foundation (SNF). G. Mistlberger greatly acknowledges the support by the Austrian Science Fund (FWF): J3343. The authors thank F. Bujard (University of Geneva) for fabricating the flow cell.

## ■ REFERENCES

- (1) Anzai, J.; Sakamura, K.; Osa, T. *J. Chem. Soc., Chem. Commun.* **1992**, 888–889.
- (2) Bakker, E.; Bühlmann, P.; Pretsch, E. *Chem. Rev.* **1997**, 97, 3083–3132.
- (3) He, H. R.; Uray, G.; Wolfbeis, O. S. *Anal. Chim. Acta* **1991**, 246, 251–257.
- (4) Lerchi, M.; Reitter, E.; Simon, W.; Pretsch, E.; Chowdhury, D. A.; Kamata, S. *Anal. Chem.* **1994**, 66, 1713–1717.
- (5) McCarrick, M.; Harris, S. J.; Diamond, D. *Analyst* **1993**, 118, 1127–1130.
- (6) Seiler, K.; Simon, W. *Sens. Actuators, B* **1992**, 6, 295–298.
- (7) Suzuki, K.; Tohda, K.; Tanda, Y.; Ohzora, H.; Nishihama, S.; Inoue, H.; Shirai, T. *Anal. Chem.* **1989**, 61, 382–384.
- (8) Toth, K.; Lan, B. T. T.; Jeney, J.; Horvath, M.; Bitter, I.; Grun, A.; Agai, B.; Toke, L. *Talanta* **1994**, 41, 1041–1049.
- (9) Wang, E. J.; Meyerhoff, M. E. *Anal. Chim. Acta* **1993**, 283, 673–682.
- (10) Lerchi, M.; Bakker, E.; Rusterholz, B.; Simon, W. *Anal. Chem.* **1992**, 64, 1534–1540.
- (11) Bakker, E.; Crespo, G.; Grygolowicz-Pawlak, E.; Mistlberger, G.; Pawlak, M.; Xie, X. *J. Chimia* **2011**, 65, 141–149.
- (12) Shiraiishi, Y.; Itoh, M.; Hirai, T. *Phys. Chem. Chem. Phys.* **2010**, 12, 13737–13745.
- (13) Davis, D. A.; Hamilton, A.; Yang, J. L.; Cremar, L. D.; Van Gough, D.; Potisek, S. L.; Ong, M. T.; Braun, P. V.; Martinez, T. J.; White, S. R.; Moore, J. S.; Sottos, N. R. *Nature* **2009**, 459, 68–72.
- (14) Monk, P. M. S.; Mortimer, R. J.; Rosseinsky, D. R. *Electrochromism Fundamentals and Applications*; VCH: Weinheim, Germany/Basel, Switzerland, 1995; p 216.
- (15) Mistlberger, G.; Crespo, G. A.; Xie, X. J.; Bakker, E. *Chem. Commun.* **2012**, 48, 5662–5664.
- (16) Xie, X. J.; Mistlberger, G.; Bakker, E. *J. Am. Chem. Soc.* **2012**, 134, 16929–16932.
- (17) Berridge, M. J.; Lipp, P.; Bootman, M. D. *Nat. Rev. Mol. Cell Biol.* **2000**, 1, 11–21.
- (18) Clapham, D. E. *Cell* **2007**, 131, 1047–1058.
- (19) Shvarev, A. *J. Am. Chem. Soc.* **2006**, 128, 7138–7139.
- (20) Emond, M.; Le Saux, T.; Maurin, S.; Baudin, J. B.; Plasson, R.; Jullien, L. *Chemistry* **2010**, 16, 8822–8831.
- (21) Emond, M.; Sun, J.; Gregoire, J.; Maurin, S.; Tribet, C.; Jullien, L. *Phys. Chem. Chem. Phys.* **2011**, 13, 6493–6499.
- (22) Kumar, S.; Hernandez, D.; Hoa, B.; Lee, Y.; Yang, J. S.; McCurdy, A. *Org. Lett.* **2008**, 10, 3761–3764.
- (23) Natali, M.; Giordani, S. *Chem. Soc. Rev.* **2012**, 41, 4010–4029.
- (24) Sakata, T.; Jackson, D. K.; Mao, S.; Marriott, G. *J. Org. Chem.* **2007**, 73, 227–233.
- (25) Wu, L. X.; Dai, Y. R.; Marriott, G. *Org. Lett.* **2011**, 13, 2018–2021.
- (26) Ellis-Davies, G. C. R. *Chem. Rev.* **2008**, 108, 1603–1613.
- (27) Berkovic, G.; Krongauz, V.; Weiss, V. *Chem. Rev.* **2000**, 100, 1741–1753.
- (28) Byrne, R.; Diamond, D. *Nat. Mater.* **2006**, 5, 421–424.
- (29) Evans, L.; Collins, G. E.; Shaffer, R. E.; Michelet, V.; Winkler, J. D. *Anal. Chem.* **1999**, 71, 5322–5327.
- (30) Minkin, V. I. *Chem. Rev.* **2004**, 104, 2751–2776.
- (31) Bühlmann, P.; Pretsch, E.; Bakker, E. *Chem. Rev.* **1998**, 98, 1593–1687.
- (32) Neupert-Laves, K.; Dobler, M. *J. Crystallogr. Spectrosc. Res.* **1982**, 12, 287–299.
- (33) Bakker, E. *Anal. Chem.* **1997**, 69, 1061–1069.
- (34) Yamamoto, H.; Shinkai, S. *Chem. Lett.* **1994**, 1115–1118.